



Probing the Chemical Complexity of Amines in the ISM: Detection of Vinylamine ($C_2H_3NH_2$) and Tentative Detection of Ethylamine ($C_2H_5NH_2$)

Shaoshan Zeng¹, Izaskun Jiménez-Serra² , Víctor M. Rivilla^{2,3} , Jesús Martín-Pintado² , Lucas F. Rodríguez-Almeida² , Belén Tercero⁴ , Pablo de Vicente⁴, Fernando Rico-Villas² , Laura Colzi^{2,3} , Sergio Martín^{5,6} , and Miguel A. Requena-Torres^{7,8}

¹ Star and Planet Formation Laboratory, Cluster for Pioneering Research, RIKEN, 2-1 Hirosawa, Wako, Saitama, 351-0198, Japan; shaoshan.zeng@riken.jp

² Centro de Astrobiología (CSIC-INTA), Ctra. Ajalvir km 4, Torrejón de Ardoz, E-28850, Madrid, Spain

³ INAF-Osservatorio Astrofisico di Arcetri, Largo E. Fermi 5, I-50125, Florence, Italy

⁴ Observatorio de Yebes (IGN), Cerro de la Palera s/n, E-19141, Guadalajara, Spain

⁵ European Southern Observatory, Alonso de Córdova 3107, Vitacura 763 0355, Santiago, Chile

⁶ Joint ALMA Observatory, Alonso de Córdova 3107, Vitacura 763 0355, Santiago, Chile

⁷ University of Maryland, College Park, MD 20742-2421, USA

⁸ Department of Physics, Astronomy and Geosciences, Towson University, MD 21252, USA

Received 2021 July 16; revised 2021 September 29; accepted 2021 October 2; published 2021 October 14

Abstract

Amines, particularly primary amines (R-NH₂), are closely related to the primordial synthesis of amino acids since they share the same structural backbone. However, only a limited number of amines has been identified in the interstellar medium, which prevents us from studying their chemistry as well as their relation to prebiotic species that could lead to the emergence of life. In this Letter, we report the first interstellar detection of vinylamine (C₂H₃NH₂) and tentative detection of ethylamine (C₂H₅NH₂) toward the Galactic center cloud G+0.693-0.027. The derived abundance with respect to H₂ is $(3.3 \pm 0.4) \times 10^{-10}$ and $(1.9 \pm 0.5) \times 10^{-10}$, respectively. The inferred abundance ratios of C₂H₃NH₂ and C₂H₅NH₂ with respect to methylamine (CH₃NH₂) are ~ 0.02 and ~ 0.008 , respectively. The derived abundance of C₂H₃NH₂, C₂H₅NH₂, and several other NH₂-bearing species are compared to those obtained toward high-mass and low-mass star-forming regions. Based on recent chemical and laboratory studies, possible chemical routes for the interstellar synthesis of C₂H₃NH₂ and C₂H₅NH₂ are discussed.

Unified Astronomy Thesaurus concepts: [Pre-biotic astrochemistry \(2079\)](#); [Interstellar molecules \(849\)](#); [Chemical abundances \(224\)](#); [Galactic center \(565\)](#)

1. Introduction

The term prebiotic molecules refers to species that are considered to be involved in the processes leading to the origin of life. From the perspective of understanding the prebiotic chemistry in the interstellar medium (ISM), primary amines have attracted much attention because they contain the same NH₂ group as those considered to be the fundamental building blocks of life (e.g., amino acids, nucleobases, nucleotides, and other biochemical compounds). Although the attempts to observe glycine (NH₂CH₂COOH), the simplest amino acid, in the ISM have not succeeded (e.g., Ceccarelli et al. 2000; Belloche et al. 2013), an increasing number of NH₂-bearing species have been reported in the last few years, which increases the chance to discover prebiotic complex organics in space. This is in fact well-demonstrated toward G+0.693-0.027 (hereafter G+0.693), a molecular cloud located within the Sgr B2 complex in the Galactic center. As revealed by the census of N-bearing species toward G+0.693 (Zeng et al. 2018), several species containing NH₂ such as cyanamide (NH₂CN), formamide (NH₂CHO), and methylamine (CH₃NH₂) have been detected with abundance $\geq 10^{-9}$. Following the search, two key precursors in the synthesis of prebiotic nucleotides, hydroxylamine (NH₂OH) and urea (NH₂CONH₂), have also been identified toward G+0.693 (Jiménez-Serra et al. 2020; Rivilla et al. 2020). The very recent discovery of by far the most complex amine, ethanolamine (NH₂CH₂CH₂OH), the simplest head group of phospholipids in cell membranes, toward G+0.693 attests the potential of this source for finding more complex molecules of prebiotic relevance (Rivilla et al. 2021). This has thus prompted us to keep hunting

for more amines in order to understand the chemical processes yielding related ingredients for life in space.

Structurally analogous to amino acids, CH₃NH₂ is the only primary amine that has been unambiguously observed toward different astronomical objects (e.g., Kaifu et al. 1974; Zeng et al. 2018; Bøgelund et al. 2019; Ohishi et al. 2019). Vinylamine (also known as ethenamine, C₂H₃NH₂) and ethylamine (C₂H₅NH₂) have not yet been reported in the ISM although the latter has been identified in multiple meteorites (Aponte et al. 2020, and references therein) and materials returned by the Stardust mission from comet 81P/Wild 2 (e.g., Glavin et al. 2008). Due to some concerns regarding the possible contamination of the stardust sample, their cometary origin could not be confirmed before the robust detection in the coma of comet 67P/Churyumov-Gerasimenko (Altwegg et al. 2016). The detection of CH₃NH₂ and C₂H₅NH₂ together with glycine in these solar system objects enhanced the probability of amino acids being formed in space. Indeed, the retrosynthesis of amino acids revealed that molecules containing the -NH₂ functional group are likely precursors of amino acids (Förstel et al. 2017). For example, CH₃NH₂ and C₂H₅NH₂ may be the major constituents of glycine and alanine (NH₂CH₃CHCOOH), respectively. According to the detailed quantum chemical calculation, C₂H₃NH₂ is the next energetically stable isomer in C₂H₅N group after E- and Z-conformer of ethanimine (CH₃CHNH; Sil et al. 2018), both of which have been detected in Sgr B2 (Loomis et al. 2013) as well as in G+0.693 (Rivilla et al. 2021, in preparation). C₂H₅NH₂ exists in two forms: anti- and gauche-conformer. The former is known to be more stable and has a higher expected intensity ratio than the latter

conformer (see Sil et al. 2018, for details). Therefore anti-C₂H₅NH₂ should be the most viable candidate for the astronomical detection in the C₂H₇N group. In this Letter, we present the first detection of C₂H₃NH₂ and tentative detection of C₂H₅NH₂ in the ISM toward G+0.693 through the identification of several rotational transitions of its millimeter spectrum.

2. Observations

We have carried out high-sensitivity spectral surveys at 7, 3, and 2 mm toward G+0.693 molecular cloud using the IRAM 30 m⁹ and Yebes 40 m¹⁰ telescopes. The observations were centered at $\alpha(J2000) = 17^{\text{h}}47^{\text{m}}22^{\text{s}}$, $\delta(J2000) = -28^{\circ}21'27''$. The position switching mode was used in all observations with the reference position located at $\Delta\alpha, \Delta\delta = -885'', 290''$ with respect to the source position. The half-power beamwidth of the IRAM 30 m and Yebes 40 m telescopes are in a range of 14''–36'' at observed frequencies between 30 GHz and 175 GHz. The intensity of the spectra was measured in units of antenna temperature, T_{A}^* as the molecular emission toward G+0.693 is extended over the beam (Zeng et al. 2020). The IRAM 30 m observations were performed in three observing runs during 2019: April 10–16, August 13–19, and December 11–15, from project numbers 172-18 (PI Martín-Pintado), 018-19 (PI Rivilla), and 133-19 (PI Rivilla). It covered spectral ranges of 71.76–116.72 GHz and 124.77–175.5 GHz. We refer to Rivilla et al. (2020) for a full description of the IRAM 30 m observations. The Yebes 40 m observations were carried out during six observing sessions in 2020 February, as part of the project 20A008 (PI Jiménez-Serra). The new Q-band (7 mm) HEMT receiver was used to allow broadband observations in two linear polarizations. The spectral coverage ranges from 31.075 GHz to 50.424 GHz. We refer to Zeng et al. (2020) and Rivilla et al. (2020) for more detailed information on the Yebes 40 m observations.

3. Analysis and Results

The line identification and analysis were carried out using the Spectral Line Identification and Modeling (SLIM) tool implemented within the MADCUBA package¹² (version 21/12/2020, Martín et al. 2019). The spectroscopic information of C₂H₃NH₂, within 0⁺ & 0⁻ (CDMS entry 43504)¹¹ was obtained from Brown et al. (1990) and Mcnaughton & Robertson (1994). And the spectroscopic information of C₂H₅NH₂, anticonformer (CDMS entry 45515) was obtained from Fischer & Botskor (1982) and Apponi et al. (2008). Table 1 summarizes the unblended or only partially blended transitions of C₂H₃NH₂ and C₂H₅NH₂ detected toward G+0.693. Note that all the C₂H₅NH₂ lines in Table 1 are a-type transitions with selection rules of $\Delta K_a = 0$ and $\Delta K_c = \pm 1$. The rotational spectrum of C₂H₃NH₂ and C₂H₅NH₂ are characterized by inversion doubling due to the large amplitude inversion motion of the NH₂ group. Each rotational energy level, specified by the rotational quantum numbers J and K , is thus split into an inversion doublet. The 0⁺ or 0⁻ in Table 1

indicate the inversion doublet from which the transition arises. For C₂H₅NH₂, the variation of upper state degeneracy and integrated intensity of the same transition is due to the spin statistical weight of 3:1 between the symmetric and antisymmetric sublevels.

The analysis was performed under the assumption of local thermodynamic equilibrium (LTE) conditions due to the lack of collisional coefficients of C₂H₃NH₂ and C₂H₅NH₂. Due to the low density of G+0.693 ($\sim 10^4$ – 10^5 cm⁻³; Zeng et al. 2020), molecules are subthermally excited in the source and hence their excitation temperatures (in a range of 5–20 K; e.g., Requena-Torres et al. 2008; Rivilla et al. 2018; Zeng et al. 2018) are significantly lower than the kinetic temperature of the source (~ 150 K; e.g., Zeng et al. 2018). However, note that the transitions of C₂H₃NH₂ and C₂H₅NH₂ are well fitted using one excitation temperature for each species. Considering the effect of line opacity, MADCUBA-SLIM generated synthetic spectra that can be compared to the observed spectra. The MADCUBA-AUTOFIT tool was then used to provide the best nonlinear least-squares LTE fit to the data using the Levenberg–Marquardt algorithm. It is important to note that not a single transition of C₂H₃NH₂ and C₂H₅NH₂ predicted by the LTE spectrum is missing in the data. To properly evaluate the line contamination by other molecules, over 300 species have been searched for in our data set. This included not only all the molecules detected toward G+0.693 in previous studies (Requena-Torres et al. 2008; Rivilla et al. 2018, 2019, 2020, 2021; Zeng et al. 2018; Jiménez-Serra et al. 2020; Rodríguez-Almeida et al. 2021), but also those reported in the ISM.¹³ The molecule blended with the transitions of C₂H₃NH₂ and C₂H₅NH₂ is listed in the last column of Table 1. We note that the line identification and fitting file used in this analysis is the same as the one used in previous works (e.g., Zeng et al. 2018; Rodríguez-Almeida et al. 2021) as well as ongoing works. Therefore, the excitation temperatures and column densities of blending species are consistent with the ones reported in all these studies.

For C₂H₃NH₂, we detect five clean transitions and four slightly blended transitions with a blending contribution of <10% (see Figure 1). For C₂H₅NH₂, only four clean transitions are reported and three are slightly blended (Figure 2). Since the clean transitions of C₂H₅NH₂ are weak (S/N = 4 in integrated intensity; Table 1), we conclude that this species is tentatively detected. The free parameters that can be fitted are molecular column density (N_{tot}), excitation temperature (T_{ex}), radial velocity (V_{LSR}), full width at half-maximum (FWHM, $\Delta\nu$), and source size (θ). For G+0.693, we assumed that the source size is extended in MADCUBA. As the algorithm did not converge when fitting C₂H₃NH₂ with all parameters left free, we fixed the FWHM and V_{LSR} to 18 km s⁻¹ and 67 km s⁻¹, respectively, by visual inspection of the most unblended lines. These values are consistent with those from many other molecules previously analyzed in G+0.693 (FWHM ~ 20 km s⁻¹, $V_{\text{LSR}} \sim 68$ km s⁻¹; Requena-Torres et al. 2008; Zeng et al. 2018; Rivilla et al. 2018, 2019, 2020; Jiménez-Serra et al. 2020; Rodríguez-Almeida et al. 2021). The resulting LTE fit gives $T_{\text{ex}} = (18 \pm 3)$ K and $N_{\text{tot}} = (4.5 \pm 0.6) \times 10^{13}$ cm⁻². In the case of C₂H₅NH₂, the V_{LSR} was fixed to 67 km s⁻¹ and the LTE fit gives $T_{\text{ex}} = (12 \pm 5)$ K, FWHM = (18 \pm 5) km s⁻¹, and $N_{\text{tot}} = (2.5 \pm 0.7) \times 10^{13}$ cm⁻².

The resulting best LTE fit to the C₂H₃NH₂ and C₂H₅NH₂ lines is shown by the red line in Figure 1 and Figure 2 while the

⁹ IRAM is supported by INSU/CNRS (France), MPG (Germany), and IGN (Spain).

¹⁰ http://rt40m.oan.es/rt40m_en.php

¹¹ Madrid Data Cube Analysis on ImageJ is a software developed at the Center of Astrobiology (CAB) in Madrid; <http://cab.inta-csic.es/madcuba/Portada.html>.

¹² Cologne Database for Molecular Spectroscopy (Endres et al. 2016); <https://cdms.astro.uni-koeln.de/classic/>

¹³ See <https://cdms.astro.uni-koeln.de/classic/molecules>.

Table 1
List of Observed Transitions of C₂H₃NH₂ and C₂H₅NH₂

Frequency (GHz)	Transition (J_{K_a}, K_c)	$\log A_{ul}$ (s ⁻¹)	g_u	E_u (K)	rms (mK)	$\int T_A^* dv$ (mK km s ⁻¹)	S/N ^a	Blending
C ₂ H ₃ NH ₂								
92.31229	5 _{0,5} -4 _{0,4} , 0 ⁺	-5.31611	11	13.3	1.2	325	46	aGg-(CH ₂ OH) ₂
92.31539	5 _{0,5} -4 _{0,4} , 0 ⁻	-5.41309	11	78.3	1.2	8		
*92.92085	5 _{2,4} -4 _{2,3} , 0 ⁺	-5.38264	11	22.4	1.3	170	22	clean
*96.51369	5 _{1,4} -4 _{1,3} , 0 ⁺	-5.27533	11	16.1	2.5	282	19	clean
112.62479	6 _{2,4} -5 _{2,3} , 0 ⁺	-5.10095	13	27.8	5.7	198	6	g-C ₂ H ₅ SH
*128.32030	7 _{0,7} -6 _{0,6} , 0 ⁺	-4.87614	15	24.7	8.7	350	7	clean
*129.92445	7 _{2,6} -6 _{2,5} , 0 ⁺	-4.89588	15	33.9	6.8	200	5	clean
*146.03934	8 _{0,8} -7 _{0,7} , 0 ⁺	-4.70420	17	31.7	2.9	316	20	clean
149.14290	8 _{3,6} -7 _{3,5} , 0 ⁺	-4.74122	17	52.4	2.9	93	6	CH ₃ C ¹³ CH
159.88701	9 _{1,9} -8 _{1,8} , 0 ⁺	-4.58763	19	40.7	5.3	241	9	C ₂ H ₅ CN
C ₂ H ₅ NH ₂								
*32.14604	2 _{1,2} -1 _{1,1} , 0 ⁻	-6.88737	15	3.4	1.1	8	4	clean
* 32.14605	2 _{1,2} -1 _{1,1} , 0 ⁺	-6.88739	45	3.4	1.1	24		
*34.04659	2 _{1,1} -1 _{1,0} , 0 ⁻	-6.81259	15	3.5	1.2	8	4	clean
*34.04662	2 _{1,1} -1 _{1,0} , 0 ⁺	-6.81261	45	3.5	1.2	25		
*49.52875	3 _{0,3} -2 _{0,2} , 0 ⁺	-6.16968	63	4.7	2.8	67	6	clean
*49.52875	3 _{0,3} -2 _{0,2} , 0 ⁻	-6.16966	21	4.7	2.8	22		
82.16878	5 _{0,5} -4 _{0,4} , 0 ⁺	-5.48528	99	11.8	2.8	109	8	¹³ CH ₃ CH ₂ OH
82.16878	5 _{0,5} -4 _{0,4} , 0 ⁻	-5.48526	33	11.8	2.8	36		
* 83.24287	5 _{2,3} -4 _{2,2} , 0 ⁺	-5.54312	99	16.4	3.1	64	4	clean
*83.24287	5 _{2,3} -4 _{2,2} , 0 ⁻	-5.54310	33	16.4	3.1	21		
84.98078	5 _{1,4} -4 _{1,3} , 0 ⁺	-5.45828	99	13.3	3.3	96	6	H ¹⁵ NCO
84.98078	5 _{1,4} -4 _{1,3} , 0 ⁻	-5.45826	33	13.3	3.3	32		
145.87174	9 _{0,9} -8 _{0,8} , 0 ⁺	-4.72105	171	35.3	2.3	56	6	S ¹⁸ O
145.87174	9 _{0,9} -8 _{0,8} , 0 ⁻	-4.72103	57	35.3	2.3	19		

Note. The following parameters are obtained from the CDMS catalog entries 43504 and 45515: frequencies, quantum numbers, upper state degeneracy (g_u), the logarithm of the Einstein coefficients ($\log A_{ul}$), and the energy of the upper levels (E_u). The derived root mean square (rms) of the analyzed spectra region, integrated intensity ($\int T_A^* dv$), signal-to-noise ratio (S/N), and the information about the species with transitions slightly blended with C₂H₃NH₂ or C₂H₅NH₂ lines are provided in the last column.

^a S/N is calculated as $(\int T_A^* dv) / [\text{rms}(\frac{\Delta\nu}{\text{FWHM}})^{0.5} \text{FWHM}]$, where $\Delta\nu$ is the spectral resolution of the data, ranging between 1.5 and 2.2 km s⁻¹. The clean transitions are denoted by an asterisk. A single common S/N is given for the overlapping transitions.

blue line indicates the best fit considering also the total contribution of the LTE emission from all the other identified molecules. Adapting the H₂ column density inferred from observations of C¹⁸O ($N_{\text{H}_2} = 1.35 \times 10^{23} \text{ cm}^{-2}$; Martín et al. 2008), the resulting abundance is $(3.3 \pm 0.4) \times 10^{-10}$ and $(1.9 \pm 0.5) \times 10^{-10}$ for C₂H₃NH₂ and C₂H₅NH₂, respectively.

4. Discussion

Figure 3 presents the abundance with respect to H₂, in decreasing order, of NH₂-bearing species detected toward G +0.693. The results are compared to those derived toward three high-mass and low-mass star-forming regions that are chemically rich, i.e., Sgr B2(N), Orion KL, and IRAS 16293-2422 B. The low abundance or nondetection of -NH₂ species may indicate that their formation is less efficient toward Orion KL and IRAS 16293-2422 B. On the other hand, the detection with abundance $>10^{-11}$ suggests G+0.693 is a prominent -NH₂ molecule repository, which allows us to study their origin as well as their chemical relation to other prebiotic molecules.

In contrast to the three compared sources, G+0.693 lacks an internal heating source responsible for the rich chemistry. The high level of molecular complexity is attributed to dust grain sputtering by low-velocity shocks ($\leq 20 \text{ km s}^{-1}$), which is driven by the possible cloud-cloud collision occurring in the Sgr B2

complex (Zeng et al. 2020). This is indicated by the high abundances of shock tracers such as HNCO and SiO (Martín et al. 2008; Rivilla et al. 2018) and the presence of molecules that are known to be formed on grain surfaces (Requena-Torres et al. 2008; Zeng et al. 2018). In addition, the abundance ratio of HC₃N/HC₅N and C₂H₃CN/C₂H₅CN derived in Zeng et al. (2018) suggested that an enhanced cosmic-ray ionization rate may also play a role in the chemistry of N-bearing species toward G +0.693. In the following section, we evaluate the possible formation routes for the amines detected toward G+0.693 and the discussed formation routes are summarized in Figure 4.

4.1. Formation of Primary Amines

Despite the low number of detections in the ISM, the CH₃NH₂ chemistry under astrophysical conditions has been studied in theoretical, experimental, and chemical modeling work. In the gas-phase, CH₃NH₂ is proposed to form via the radiative association between ammonia (NH₃) and the methyl radical cation (CH₃⁺) followed by recombination dissociation (Herbst 1985). On the grain surfaces, experimental work demonstrated that CH₃NH₂ can form via sequential hydrogenation of hydrogen cyanide (HCN): HCN → CH₂NH → CH₃NH₂ (Theule et al. 2011). Alternatively, the gas-grain chemical model by Garrod et al. (2008) has suggested that CH₃NH₂ is formed by simple addition

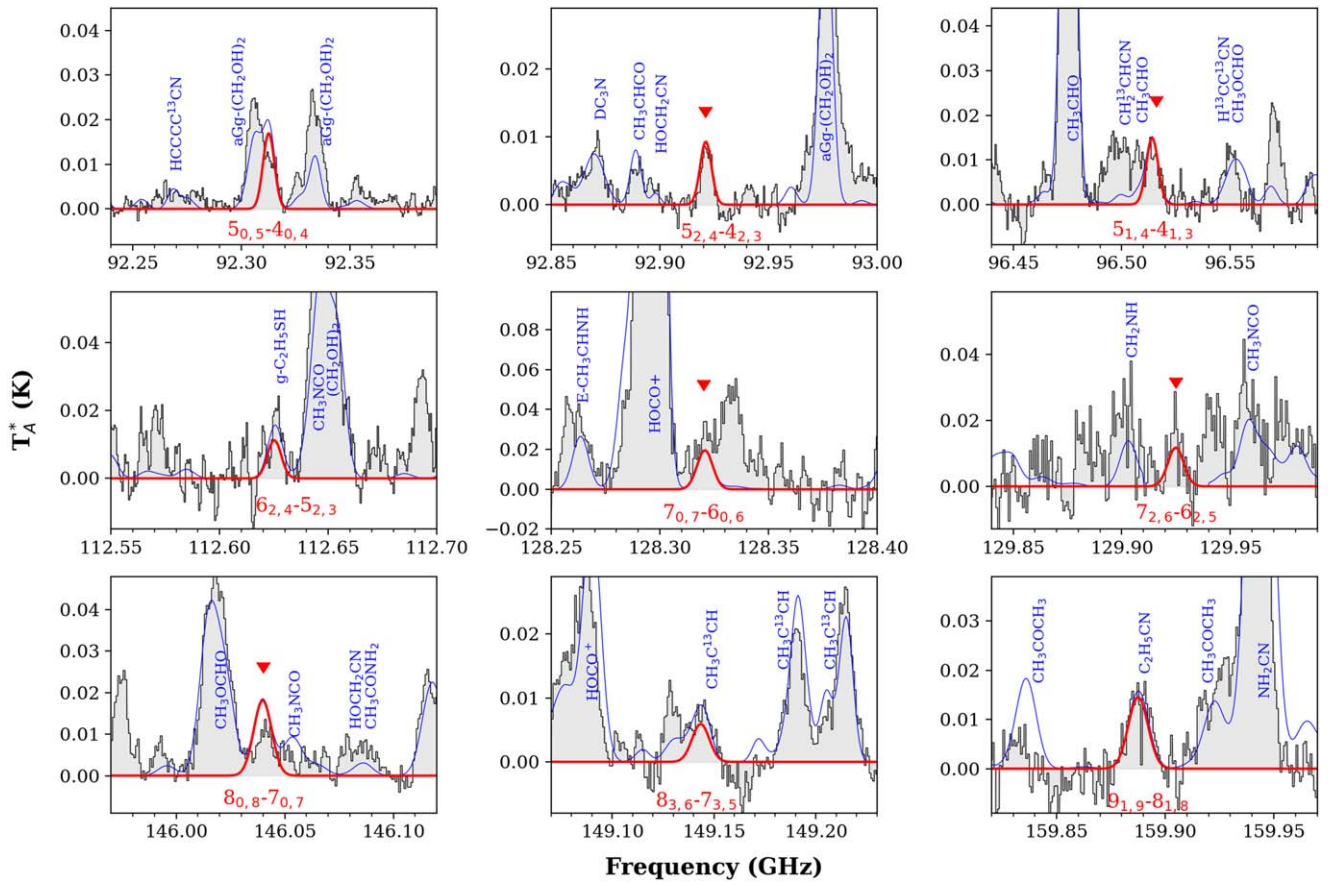


Figure 1. Unblended or only slightly blended transitions of $C_2H_5NH_2$ detected toward G+0.693. The red line shows the best LTE fit to the $C_2H_5NH_2$ lines while the blue line shows the total contribution, including the emission from other molecular species (labeled) identified in G+0.693. The cleanest detected transitions are denoted by a red \blacktriangledown .

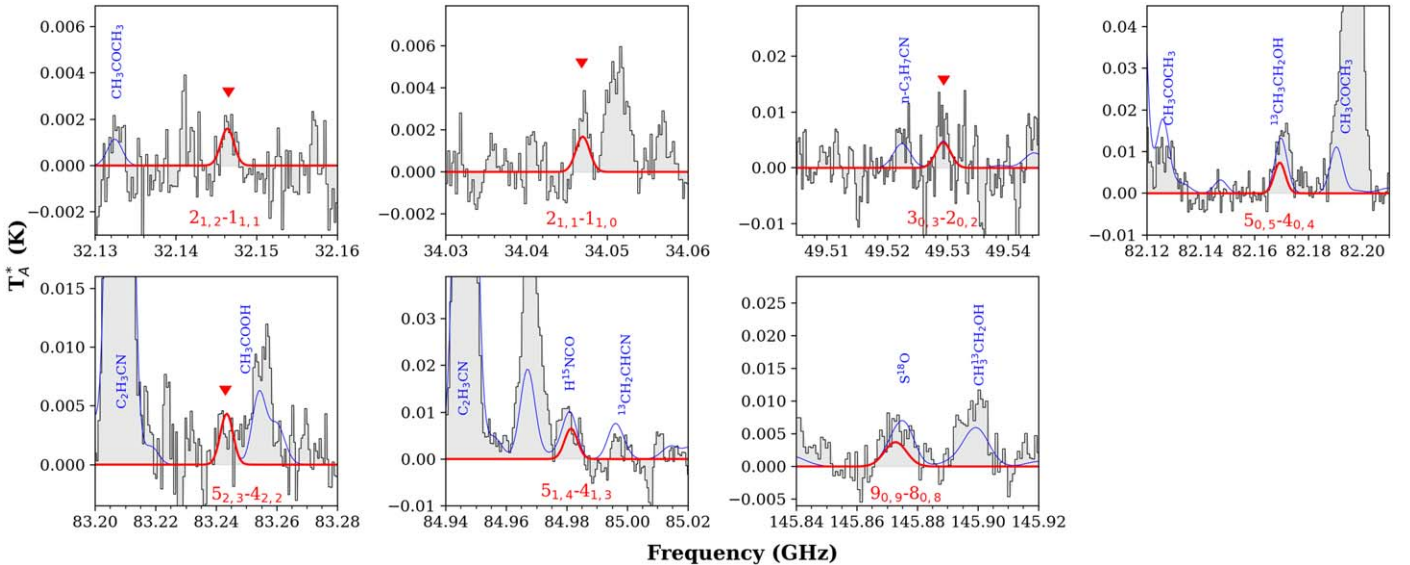


Figure 2. Unblended or only slightly blended transitions tentatively identified for $C_2H_5NH_2$ toward G+0.693. The cleanest transitions are denoted by a red \blacktriangledown .

of CH_3 from CH_4 to azanyl radical (NH_2) from NH_3 during warm-up phases. This radical–radical recombination has recently been studied in laboratory ice simulations revealing that CH_3NH_2 can be synthesized in irradiated ices composed of CH_4 and NH_3 (Kim & Kaiser 2011; Förstel et al. 2017) but also in cold and quiescent molecular clouds (Ioppolo et al. 2021). On the

contrary, little is known about the chemistry of $C_2H_5NH_2$ and $C_2H_5NH_2$.

$C_2H_5NH_2$ —Although there are no chemical routes included in current astrochemical databases, different formation mechanisms of $C_2H_5NH_2$ have been discussed in the literature. For instance, the addition of the CH_3 radical to CH_2NH followed

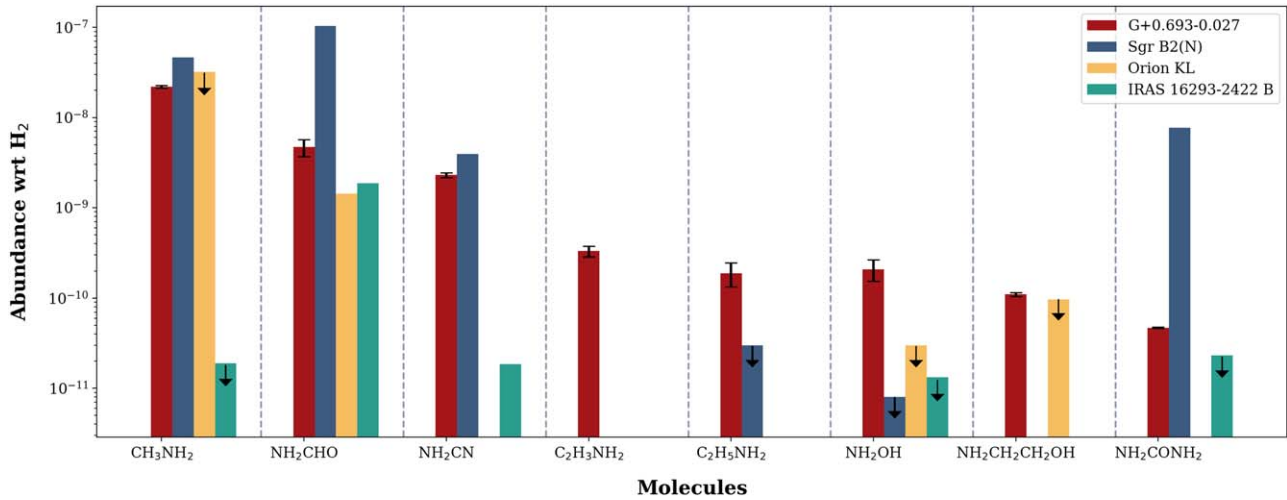


Figure 3. Derived abundance of NH_2 -bearing species with respect to H_2 toward G+0.693-0.027, Sgr B2(N), Orion KL, and IRAS 16293-2422 B. For G+0.693-0.027 ($N(\text{H}_2) = 1.35 \times 10^{23} \text{ cm}^{-2}$; Martín et al. 2008), molecular column densities are obtained from this work, Zeng et al. (2018), Jiménez-Serra et al. (2020), Rivilla et al. (2020), and Rivilla et al. (2021). For IRAS 16293-2422 B ($N(\text{H}_2) = 2.8 \times 10^{25} \text{ cm}^{-2}$; Martín-Doménech et al. 2017), molecular column densities are from Martín-Doménech et al. (2017), Ligterink et al. (2018), and Jiménez-Serra et al. (2020). For Sgr B2(N), CH_3NH_2 , NH_2CHO , and NH_2CN are from Belloche et al. (2013) with $N(\text{H}_2) = 1.3 \times 10^{25} \text{ cm}^{-2}$ (Belloche et al. 2008); the abundance of $\text{C}_2\text{H}_5\text{NH}_2$ and the upper limit of NH_2OH are taken directly from Apponi et al. (2008) and Pulliam et al. (2012), respectively; NH_2CONH_2 is derived from Belloche et al. (2019) by assuming Sgr B2(N1S) has the same $N(\text{H}_2) = 3.5 \times 10^{24} \text{ cm}^{-2}$ (Li et al. 2021) as Sgr B2 (N1E). For Orion KL, the column density of CH_3NH_2 and $N(\text{H}_2) = 3.1 \times 10^{23} \text{ cm}^{-2}$ are from Pagani et al. (2017); NH_2CHO is from Motiyenko et al. (2012) with $N(\text{H}_2) = 4.2 \times 10^{23} \text{ cm}^{-2}$ (Tercero et al. 2010); upper limits of NH_2OH and $\text{NH}_2\text{CH}_2\text{CH}_2\text{OH}$ are from Pulliam et al. (2012) and Wirström et al. (2007), respectively, with $N(\text{H}_2) = 7.0 \times 10^{23} \text{ cm}^{-2}$ (Womack et al. 1992).

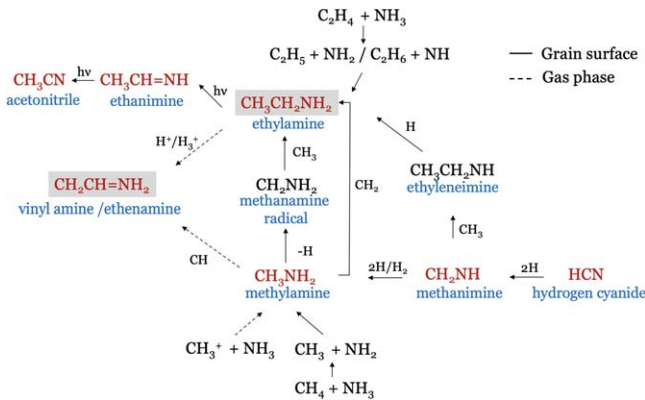


Figure 4. Summary of the chemical routes proposed for the formation of $\text{C}_2\text{H}_5\text{NH}_2$ and $\text{C}_2\text{H}_3\text{NH}_2$ in the ISM. The molecular species in red are those that have been detected toward G+0.693. The solid arrows denote surface chemistry reactions and dashed arrows denote gas-phase chemistry.

by hydrogenation of the resulting product would produce $\text{C}_2\text{H}_5\text{NH}_2$ on grain surfaces (Bernstein et al. 1995); the photochemistry of a mixture of ethylene (C_2H_4) and NH_3 in which $\text{C}_2\text{H}_5\text{NH}_2$ is formed from radical-radical reaction of the ethyl radical (C_2H_5) with NH_2 (Danger et al. 2011, and references therein). Reactions of CH_3NH_2 with carbene (CH_2) or ethane (C_2H_6) with nitrene (NH) are also expected to form $\text{C}_2\text{H}_5\text{NH}_2$, but with lower probability (Förstel et al. 2017). More recently, experimental simulation of interstellar ice analogs containing CH_3NH_2 revealed that $\text{C}_2\text{H}_5\text{NH}_2$ can be formed efficiently from CH_3 and methanimine radical (CH_2NH_2 ; Carrascosa et al. 2021).

In addition to the aforementioned formation pathways, one might also expect $\text{C}_2\text{H}_5\text{NH}_2$ to be formed through the same mechanism as suggested for CH_3NH_2 : successive hydrogenation starting from acetonitrile (CH_3CN): $\text{CH}_3\text{CN} \rightarrow \text{CH}_3\text{CHNH} \rightarrow \text{C}_2\text{H}_5\text{NH}_2$. However, CH_3CN has been proposed to be a product

of the surface chemistry of CH_3NH_2 (Carrascosa et al. 2021). Furthermore, laboratory work showed that CH_3CN does not react with H atoms between 10 and 60 K (Nguyen et al. 2019). Considering the temperature of dust grains in G+0.693 is $T_{\text{dust}} \leq 30 \text{ K}$ (Zeng et al. 2018, and reference therein), this proposed hydrogenation leading to $\text{C}_2\text{H}_5\text{NH}_2$ is unlikely to occur on dust grains in G+0.693. Based on the reaction rate coefficients provided in Sil et al. (2018), $\text{C}_2\text{H}_5\text{NH}_2$ is less likely produced in the same hydrogenation reaction in the gas phase due to its low efficiency at typical kinetic temperature in Galactic center clouds, $T_{\text{kin}} = 50\text{--}120 \text{ K}$ (Zeng et al. 2018, and reference therein). To our best knowledge, with no other possible gas-phase reaction to form $\text{C}_2\text{H}_5\text{NH}_2$, this species likely forms on the surface of dust grains in G+0.693. Regardless of the chemical formation route on grains, the sputtering of grain icy mantles by large-scale low-velocity ($\leq 20 \text{ km s}^{-1}$) shocks in G+0.693 would release $\text{C}_2\text{H}_5\text{NH}_2$ into gas phase from grains (see, e.g., Martín et al. 2008; Requena-Torres et al. 2008; Zeng et al. 2020).

$\text{C}_2\text{H}_3\text{NH}_2$ —With the available reaction rate coefficients in the Kinetic Database for Astrochemistry (Wakelam et al. 2012), $\text{C}_2\text{H}_3\text{NH}_2$ is proposed to form from the reaction between the CH radical and CH_3NH_2 in the gas-phase, most efficient at temperatures $T = 50\text{--}200 \text{ K}$. With $T_{\text{kin}} = 50\text{--}120 \text{ K}$, $\text{C}_2\text{H}_3\text{NH}_2$ is thus expected to be formed efficiently via this pathway in G+0.693. In particular, CH_3NH_2 is found to be abundant ($\sim 10^{-8}$; Zeng et al. 2018) in G+0.693, which would be readily available for this chemical reaction to proceed. Another possible gas-phase formation route is through the reaction involving $\text{C}_2\text{H}_5\text{NH}_2 + \text{H}^+$ or H_3^+ followed by recombination dissociation, analogous to the formation of $\text{C}_2\text{H}_3\text{CN}$ from $\text{C}_2\text{H}_5\text{CN}$ proposed by Caselli et al. (1993). As discussed in Zeng et al. (2018) for -CN group species, this ion-molecule gas-phase reaction can be efficient thanks to (i) the presence of high cosmic-ray ionization rate in the Galactic center and (ii) the relatively low densities of $\sim 10^4 \text{ cm}^{-3}$ of G+0.693. This, and the fact that similar abundance ratios are found

for $C_2H_3CN/C_2H_5CN = 2.2 \pm 0.3$ and $C_2H_3NH_2/C_2H_5NH_2 = 1.7 \pm 0.5$ toward G+0.693, makes this formation route plausible.

On the grain surface, $C_2H_3NH_2$ might be a photoproduct of $C_2H_5NH_2$ (Hamada et al. 1984). But recent experimental investigation showed that its isomer, ethanimine (CH_3CHNH), appears to be the primary product of photolysis of $C_2H_5NH_2$ (Danger et al. 2011). This has also been recently found by Carrascosa et al. (2021), who even synthesized large N-heterocycles in interstellar ice analogs under UV radiation. We thus propose that the formation of $C_2H_3NH_2$ likely occurs in the gas phase toward G+0.693 although further theoretical or laboratory work is needed to determine the rate constant of the reaction $C_2H_5NH_2 + H^+/H_3^+$.

In summary, we report the discovery of two new amines in the ISM: $C_2H_3NH_2$ and tentatively $C_2H_5NH_2$. The abundance ratios with respect to CH_3NH_2 are ~ 0.02 and ~ 0.008 , i.e., about a factor >10 . This trend has been found for other species such as ethanol (with respect to methanol) or ethyl cyanide (with respect to CH_3CN ; Zeng et al. 2018; Rodríguez-Almeida et al. 2021). Primary amines are known to be involved in the synthesis of proteinogenic alpha-amino acids (Förstel et al. 2017). Therefore, their discovery provides crucial information about the connection between interstellar chemistry and the prebiotic material found in meteorites and comets.

The authors wish to thank the referees for constructive comments that significantly improved the paper. We are grateful to the IRAM 30 m and Yebes 40 m telescope staff for help during the different observing runs. IRAM is supported by the National Institute for Universe Sciences and Astronomy/National Center for Scientific Research (France), Max Planck Society for the Advancement of Science (Germany), and the National Geographic Institute (IGN) (Spain). The 40 m radio telescope at Yebes Observatory is operated by the IGN, Ministerio de Transportes, Movilidad y Agenda Urbana. This study is supported by a Grant-in-Aid from the Ministry of Education, Culture, Sports, Science, and Technology of Japan (20H05845) and by a RIKEN pioneering Project (Evolution of Matter in the Universe). We also acknowledge partial support from the Spanish National Research Council (CSIC) through the i-Link project number LINKA20353. I.J.-S. and J.M.-P. have received partial support from the Spanish State Research Agency through project number PID2019-105552RB-C41. V.M.R., L.R.-A., and L.C. have received funding from the Comunidad de Madrid through the Atracción de Talento Investigador (Doctores con experiencia) Grant (COOL: Cosmic Origins Of Life; 2019-T1/TIC-15379).

ORCID iDs

Izaskun Jiménez-Serra  <https://orcid.org/0000-0003-4493-8714>
 Víctor M. Rivilla  <https://orcid.org/0000-0002-2887-5859>
 Jesús Martín-Pintado  <https://orcid.org/0000-0003-4561-3508>
 Lucas F. Rodríguez-Almeida  <https://orcid.org/0000-0002-9785-703X>
 Belén Tercero  <https://orcid.org/0000-0002-4782-5259>
 Fernando Rico-Villas  <https://orcid.org/0000-0002-5351-3497>
 Laura Colzi  <https://orcid.org/0000-0001-8064-6394>
 Sergio Martín  <https://orcid.org/0000-0001-9281-2919>

References

- Altwegg, K., Balsiger, H., Bar-Nun, A., et al. 2016, *SciA*, 2, e1600285
 Aponte, J. C., Elsila, J. E., Hein, J. E., et al. 2020, *M&PS*, 55, 2422
 Apponi, A. J., Sun, M., Halfen, D. T., Ziurys, L. M., & Müller, H. S. P. 2008, *ApJ*, 673, 1240
 Belloche, A., Garrod, R. T., Müller, H. S. P., et al. 2019, *A&A*, 628, A10
 Belloche, A., Menten, K. M., Comito, C., et al. 2008, *A&A*, 482, 179
 Belloche, A., Müller, H. S. P., Menten, K. M., Schilke, P., & Comito, C. 2013, *A&A*, 559, A47
 Bernstein, M. P., Sandford, S. A., Allamandola, L. J., Chang, S., & Scharberg, M. A. 1995, *ApJ*, 454, 327
 Bøgelund, E. G., McGuire, B. A., Hogerheijde, M. R., van Dishoeck, E. F., & Ligterink, N. F. W. 2019, *A&A*, 624, A82
 Brown, R. D., Godfrey, P. D., Kleibomer, B., Pierlot, A. P., & McNaughton, D. 1990, *JMoSp*, 142, 195
 Carrascosa, H., González Díaz, C., Muñoz Caro, G. M., Gómez, P. C., & Sanz, M. L. 2021, arXiv:2106.05622
 Caselli, P., Hasegawa, T. I., & Herbst, E. 1993, *ApJ*, 408, 548
 Ceccarelli, C., Loinard, L., Castets, A., Faure, A., & Lefloch, B. 2000, *A&A*, 362, 1122
 Danger, G., Bossa, J. B., de Marcellus, P., et al. 2011, *A&A*, 525, A30
 Endres, C. P., Schlemmer, S., Schilke, P., Stutzki, J., & Müller, H. S. P. 2016, *JMoSp*, 327, 95
 Fischer, E., & Botskor, I. 1982, *JMoSp*, 91, 116
 Förstel, M., Bergantini, A., Maksyutenko, P., Góbi, S., & Kaiser, R. I. 2017, *ApJ*, 845, 83
 Garrod, R. T., Widicus Weaver, S. L., & Herbst, E. 2008, *ApJ*, 682, 283
 Glavin, D. P., Dworkin, J. P., & Sandford, S. A. 2008, *M&PS*, 43, 399
 Hamada, Y., Hashiguchi, K., Tsuboi, M., Koga, Y., & Kondo, S. 1984, *JMoSp*, 105, 93
 Herbst, E. 1985, *ApJ*, 292, 484
 Ioppolo, S., Fedoseev, G., Chuang, K. J., et al. 2021, *NatAs*, 5, 197
 Jiménez-Serra, I., Martín-Pintado, J., Rivilla, V. M., et al. 2020, *AsBio*, 20, 1048
 Kaifu, N., Morimoto, M., Nagane, K., et al. 1974, *ApJL*, 191, L135
 Kim, Y. S., & Kaiser, R. I. 2011, *ApJ*, 729, 68
 Li, J., Wang, J., Lu, X., et al. 2021, arXiv:2108.05001
 Ligterink, N. F. W., Calcutt, H., Coutens, A., et al. 2018, *A&A*, 619, A28
 Loomis, R. A., Zaleski, D. P., Steber, A. L., et al. 2013, *ApJL*, 765, L9
 Martín, S., Martín-Pintado, J., Blanco-Sánchez, C., et al. 2019, *A&A*, 631, A159
 Martín, S., Requena-Torres, M. A., Martín-Pintado, J., & Mauersberger, R. 2008, *ApJ*, 678, 245
 Martín-Doménech, R., Rivilla, V. M., Jiménez-Serra, I., et al. 2017, *MNRAS*, 469, 2230
 Mcnaughton, D., & Robertson, E. G. 1994, *JMoSp*, 163, 80
 Motiyenko, R. A., Tercero, B., Cernicharo, J., & Margulès, L. 2012, *A&A*, 548, A71
 Nguyen, T., Fourné, I., Favre, C., et al. 2019, *A&A*, 628, A15
 Ohishi, M., Suzuki, T., Hirota, T., Saito, M., & Kaifu, N. 2019, *PASJ*, 71, 86
 Pagani, L., Favre, C., Goldsmith, P. F., et al. 2017, *A&A*, 604, A32
 Pulliam, R. L., McGuire, B. A., & Remijan, A. J. 2012, *ApJ*, 751, 1
 Requena-Torres, M. A., Martín-Pintado, J., Martín, S., & Morris, M. R. 2008, *ApJ*, 672, 352
 Rivilla, V. M., Jiménez-Serra, I., Martín-Pintado, J., et al. 2021, *PNAS*, 118, 2101314118
 Rivilla, V. M., Jiménez-Serra, I., Zeng, S., et al. 2018, *MNRAS*, 475, L30
 Rivilla, V. M., Martín-Pintado, J., Jiménez-Serra, I., et al. 2019, *MNRAS*, 483, L114
 Rivilla, V. M., Martín-Pintado, J., Jiménez-Serra, I., et al. 2020, *ApJL*, 899, L28
 Rodríguez-Almeida, L. F., Jiménez-Serra, I., Rivilla, V. M., et al. 2021, *ApJL*, 912, L11
 Sil, M., Gorai, P., Das, A., et al. 2018, *ApJ*, 853, 139
 Tercero, B., Cernicharo, J., Pardo, J. R., & Goicoechea, J. R. 2010, *A&A*, 517, A96
 Theule, P., Borget, F., Mispelaer, F., et al. 2011, *A&A*, 534, A64
 Wakelam, V., Herbst, E., Loison, J. C., et al. 2012, *ApJS*, 199, 21
 Wirstrom, E. S., Bergman, P., Hjalmarsen, Å., & Nummelin, A. 2007, *A&A*, 473, 177
 Womack, M., Ziurys, L. M., & Wyckoff, S. 1992, *ApJ*, 393, 188
 Zeng, S., Jiménez-Serra, I., Rivilla, V. M., et al. 2018, *MNRAS*, 478, 2962
 Zeng, S., Zhang, Q., Jiménez-Serra, I., et al. 2020, *MNRAS*, 497, 4896